TUTORIAL • **OPEN ACCESS**

Electron–molecule collision calculations: a primer

OPEN ACCESS
IOP Publishing
Journal of Physics B: Atomic, Molecular and Optical Physics
J. Phys. B: At. Mol. Opt. Phys. **57** (2024) 233001 (17pp)
https://doi.org/10.1088/1361-6455/ad4243

Tutorial

Electron–molecule collision calculations: a primer

Jonathan Tennyson

Department of Physics and Astronomy, University College London, WC1E 6BT London, United Kingdom
Quantemol Ltd, 320 City Road, The Angel, London EC1V 2NZ, United Kingdom

E-mail: j.tennyson@ucl.ac.uk

Received 26 January 2024, revised 17 March 2024
Accepted for publication 23 April 2024
Published 7 November 2024

Abstract

Electron–molecule collisions drive many natural phenomena and are playing an increasing role in modern technologies. Over recent years, studies of the collision processes have become increasingly driven by quantum mechanical calculations rather than experiments. This tutorial surveys important issues underlying the physics and theoretical methods used to study electron–molecule collisions. It is aimed at nonspecialists with suitable references for further reading for those interested and pointers to software for those wanting to perform actual calculations.

Keywords: electron–molecule scattering, *ab initio*, R-matrix, dissociative attachment, dissociative recombination, electron impact excitation

1. Introduction

Collisions of electrons with molecules occur in a number of natural environments ranging from the Earth's ionosphere to the interstellar medium and from lightning bolts to radiation damage within living organisms. Perhaps even more importantly, electron–molecule collisions are widely used in modern technologies where low-temperature plasmas are used for a wide range of etching, coating and deposition processes that drive much of modern industry. These collisions also occur in spark plugs, drive many lasers, feature strongly in spacecraft re-entry physics and are employed in radiation therapy to fight cancer. The study of electron–molecule collisions thus not only probes the fundamental physics of the process but can also provide important information, which can help our understanding and models of the processes listed above and many others.

Early data on electron–molecule collisions came almost entirely from experimental studies; see the excellent review of collisions with diatomic molecules by Brunger and Buckman (2002) for example. Of course, experiment remains a means whereby detailed and accurate results can be obtained. However, over the past few decades theory has become the predominant provider of information on electron–molecule collisions. As discussed by Bartschat and Kushner (2016), there are a number of reasons for this, such as:

- The need for complete data sets of collision processes as input for models to interpret the phenomena listed above.
- The extreme difficulty of performing collision experiments on unstable species and radicals and the few successful attempts to perform these experimental studies (Maddern *et al* 2008, Brunton *et al* 2013) have provided only very limited information.

- The extreme difficulty of performing electron collision experiments where the target is in a known excited state; again there are examples of such studies, such as Johnstone *et al* (1999), but they can usually only be achieved under special circumstances and provide limited information.
- There are processes that are important but not conducive to experimental study. One such example discussed below is the rotational excitation of molecular ions, which is important for astrophysics.
- There are issues with correctly measuring forward scattering in systems with dipole moments; again this issue is discussed below.
- Some applications, such as fusion, require data on isotopically substituted species such as HT, DT and T_2. Under these circumstances, developing a theoretical model for the parent isotopologue (here H_2), which can be benchmarked against experiment, and then using it for the other species, is the most practical approach.

Finally, it should be noted that experiments are in general much slower and much more expensive than theory. All this has led to a trend towards experiments providing benchmark measurements and being used to search for novel phenomena, while theory is used to satisfy data needs for a wide range of applications.

This tutorial review is designed to provide a brief introduction to the field and pointers to the literature where those interested can gain a deeper understanding. Topics covered include the different physics encountered during collisions in different energy regimes, a taste of the quantum mechanical formalism used to treat electron–molecule collisions, model building and available methods for solving the problem, the different processes that are initiated in these collisions and finally data compilations.

2. Energy ranges

Before considering actual theoretical methods, it is worth considering the effects of different energy ranges on the scattering process.

Most work (and most of this tutorial review) focuses on low-energy collisions. This means that the impacting electron has insufficient energy to ionize the molecular target, i.e. the collision energy is below the ionization potential of the molecular target, which typically lies somewhere in the 10–15 eV range. This is known as the low-energy regime. In the low-energy regime, the electron approaches the molecule slowly enough that when it is close to the molecular target it cannot be distinguished from the electrons in that target. This means that exchange interactions need to be explicitly accounted for and the interactions are therefore non-local, although interaction potentials, including the so-called exchange potentials (Hara 1967), are sometimes used to represent electron collisions in this regime (see, for example Gianturco and Jain (1986)).

One key result, which has stimulated much work on low-energy collisions, was the discovery by Boudaïffa *et al* (2000) that high-energy particles, including electrons, create a shower of low (sub 10 eV) electrons in biological systems. It is now accepted that collisions of these low-energy electrons, which get trapped in quasi-bound resonance states (see below), provide the primary mechanism for radiation damage in living systems (Sanche 2009). This has led to considerable study of low-energy electron collisions with biologically relevant molecules and molecular clusters (Gorfinkiel and Ptasinska 2017).

The high energy regime, which starts at collision energies somewhere between 50 and 100 eV, is where the electron moves so fast that the exchange process can be treated approximately, or even neglected completely, without significant loss of accuracy. Instead, these collisions can be treated using simplified methods; these include the use of the Born approximation (Tanaka *et al* 2016), which is in essence perturbation theory formulated for continuum state problems, and the distorted wave approximation (Toshima *et al* 1987), an extension of the Born approximation, which accounts for higher-order and multiple scattering effects. The relative unimportance of exchange interactions at high energy means that the use of model potentials can also yield good results for high-energy electron scattering calculations. There are two forms of potential scattering, which are currently fairly widely used, namely the spherical complex optical potential (SCOP) (Jain 1987) and the independent atom model with the screening-corrected additivity rule including interference effects (IAM-SCAR+I) (Blanco *et al* 2016) methods. In the SCOP method, the real part of the potential models elastic scattering while the complex part models all inelastic processes, which are not differentiated in the calculation. The IAM-SCAR+I method starts from the notion that molecules are a collection of atoms and electron–molecule scattering can be modelled by considering the sum over electron atom events. As the complexity of the acronym suggests, a number of correction terms are usually included.

Electron-impact ionization is a special case of high-energy scattering since there are a number of specific and rather successful semi-empirical theories available for modelling this process. Electron impact ionization is well treated by semi-empirical methods such as BEB (Binary Encounter Bethe) (Kim and Rudd 1994) and Deutsch-Märk (Deutsch *et al* 2000) methods. These methods require only information about the target molecule to provide reliable estimates of the electron impact single-ionization cross-section of a molecule; figure 1 shows an example. BEB calculations, in particular, are generally found to give predicted cross-sections within about 10% of the measured ones.

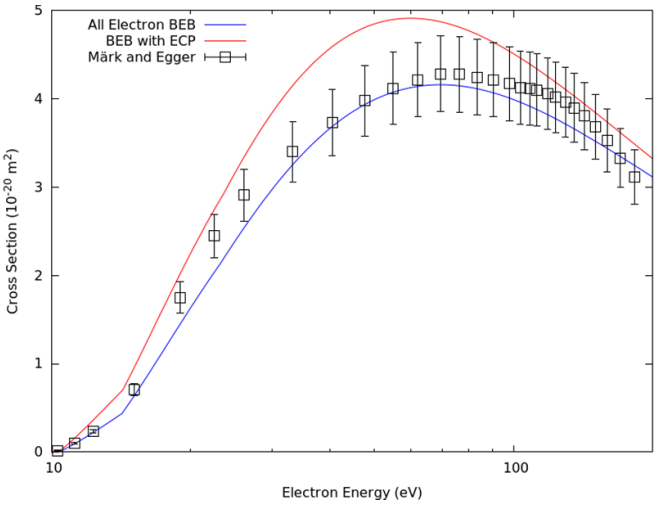

Figure 1. Electron impact ionization cross-section of phosphine (PH_3) as measured by Märk and Egger (1977) and computed using the BEB approximation with and without the use of an effective core potential (ECP) for the P atom by Graves *et al* (2021).

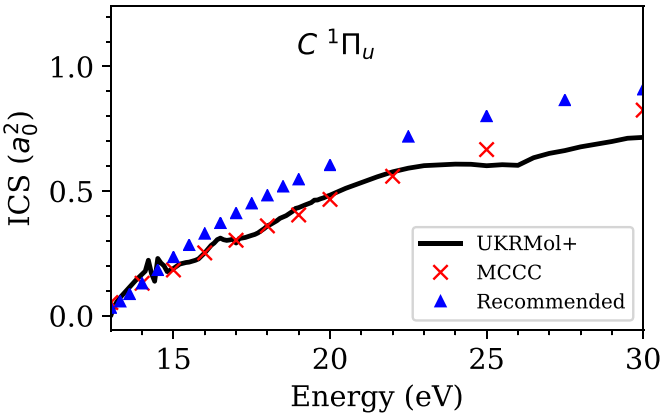

Figure 2. Electron impact cross-section for the excitation of H_2 from its $X\ ^1\Sigma_g^+$ ground state to the $C\ ^1\Pi_u$ electronically excited state. CCC and R-matrix (UKRmol+) calculations from Meltzer *et al* (2020) are compared with the measured values of Liu *et al* (1998) recommended by Yoon *et al* (2008). Note that this is a dipole-allowed transition, which means that there is a non-zero transition dipole moment linking the $X\ ^1\Sigma_g^+$ and $C\ ^1\Pi_u$ electronic states.

At even higher energies there is a regime where the electron moves at relativistic energies. This situation is less common than lower-energy scattering but does occur when high-energy cosmic rays hit the top of the Earth's atmosphere resulting in a shower of lower-energy electrons caused by collisions with atmospheric molecules. Relativistic scattering will not be considered further.

From a theoretical perspective, the hardest regime to study is the intermediate energy regime, which starts just below the ionization potential of the target and continues to 50 eV or so. This regime spans the region where the target can be excited into a potentially infinite number of bound states or ionized into a set of continuum states represented by an ionized target and a free electron. Standard low-energy methods, which often use an expansion over target states generally known as a close-coupling (CC) expansion (see below), do not readily transfer to a regime where these expansions become infinite. This is the intermediate energy regime where the greatest recent theoretical progress has been made based on the use of quasi-complete CC expansions. The most impressive results have been obtained using the CCC (convergent close-coupling) method (Zammit *et al* 2017), which, however, is limited to simple, few-active electron targets. The R-matrix with pseudo-states (RMPS) method for molecules (Gorfinkiel and Tennyson 2004, 2005) is in principle more general, but becomes very computationally expensive even for relatively small molecules (Halmová and Tennyson 2008). The RMPS and CCC methods, for which more technical details are given below, have been benchmarked against each other for electron collisions with H_2 (Meltzer *et al* 2020) giving comparable results and, interestingly, suggesting that some of the measured recommended cross-sections (Yoon *et al* 2008) for this relatively simple and fundamental system are not reliable; figure 2 gives an example.

3. (Brief) formalism

3.1. Overview

Theoretical calculations of electron–molecule scattering are based on approximations made to a rigorous, quantum mechanical formulation of the problem. As discussed in the previous section, these approximations vary according to the collision energy being considered. Some of the concepts discussed below are general, but the focus of most of the discussion will be on treating the important low- to intermediate-energy region.

The starting point for all the calculations described below is the Born–Oppenheimer approximation, which assumes that since the electrons are much lighter than the atomic nuclei, they can relax instantaneously to any nuclear motion. Within this approximation the treatment of electron scattering problems involves considering scattering from a molecule with a fixed geometry.

Before giving any mathematical details, it is worth considering the dominant interactions that need to be considered in an electron–molecule collision. To do this, it is worth dividing space into two regions: an inner region, which encloses the charge distribution of the N-electron target molecule and an outer region where one can assume the target wavefunction/charge density is zero. The boundary between these two regions is problem-dependent but is

typically taken to be in the range of 10–15 a_0. The actual division of the space between the inner and outer regions is the formal basis of the R-matrix method, discussed in the next section. However, in practice most other low-energy scattering methods make use of the concept of dividing space into different regions in their practical implementation since it yields both major computational efficiencies and physical insight.

In the inner region, the scattering electrons overlap the charge cloud of the target molecules. This means that in this region the electrons cannot be distinguished from the target electrons and the full set of $N+1$ electrons have to obey the Pauli principle; that is, the scattering wavefunction must be antisymmetric to interchange with any pair of these electrons. A consequence of this antisymmetrization is the presence of exchange interactions, which act as an important repulsive force at low energies. The overlap between the target and scattering electrons means that electron correlation, often referred to as polarization by scientists doing scattering calculations, is also important. The inner region problem has strong similarities to the electronic structure problem routinely tackled by quantum chemistry programmes such as Molpro (Werner *et al* 2012). Similar to wavefunction formulations of the quantum chemistry problem, the treatment of the exchange interaction is built into the formalism from the start by ensuring that all wavefunctions are fully antisymmetrized. Conversely, calculations usually start from models that neglect the electron-correlation, such as the Hartree–Fock (HF) approximation, and correlation effects are then treated by systematically improving on these models by a variety of methods but are rarely captured in full, with the exception of few-electron problems for which full configuration interaction treatments are possible, see Darby-Lewis *et al* (2017) for example.

At long range the interaction between the electron and the target can be formulated in terms of target moments, such as charge, dipole, quadrupole, etc, as well as its static polarizability. In this formulation there is no need to explicitly consider the wavefunction of the target as the uniquely identified scattering electron can be assumed to move in various long-range potentials. The standard way of solving this problem is to use a so-called partial wave expansion, which represents the scattering wavefunction as a product of a radial and an angular function of the form $f_{i\ell m}(r)Y_{\ell m}(\theta,\phi)$ where $\underline{r}=(r,\theta,\phi)$ is the vector representing the position of the scattering electron relative to the target centre-of-mass. The angular behaviour is represented by the spherical harmonic $Y_{\ell m}$ which represent s ($\ell=0$), p ($\ell=1$), d($\ell=2$), … partial waves. This expansion is particularly useful for low-energy scattering since it often converges rapidly and the number of partial waves that need to be explicitly considered is small; typically ℓ is truncated at about 5. The exceptions to this case are where there is a long-range potential; the inclusion of high partial waves for systems with dipoles is discussed below. Each unique asymptotic combination of $f_{i\ell m}(r)Y_{\ell m}(\theta,\phi)$ is known as a channel. In contrast to electron-atom scattering, electron–molecule scattering has many degenerate channels for which the asymptotic energy of a given set of channels is the same.

3.2. Asymptopia

When deriving a form for the wavefunction for electron–molecule scattering, $\Psi^{(N+1)}\left(\underline{r}_1\ldots\underline{r}_N,\underline{r}_{N+1}\right)$, it is simplest to start from the general form that applies at large separations ($r_{N+1}\rightarrow\infty$) between the electron and the target:

$$\Psi^{(N+1)}=\sum_{ij}a_{ij}\phi_i^N\left(\underline{r}_1\ldots\underline{r}_N\right)F_{ij}\left(r_{N+1}\right)Y_{\ell m}\left(\hat{r}_{N+1}\right), \qquad (1)$$

where $\phi_i^N(\underline{r}_1\ldots\underline{r}_N)$ represents the wavefunction of the N-electron target state i, $Y_{\ell m}$ are the spherical harmonic and F_{ij} radial function representing the continuum electron discussed above, and $\underline{r}_i=(r_i,\hat{r}_i)=(r_i,\theta_i,\phi_i)$ is the coordinate of the ith electron.

For simplicity, equation (1) and the more complete equation (7) below do not include any representation of how the spins of the electrons are coupled. For a spin singlet, spin degeneracy $2S+1=1$ target state the resulting $N+1$ electron system is a doublet. In all other cases, where $2S+1>1$ for the target, there are always two possible spin states formed in the collision system, which correspond to a spin multiplicity of $2S$ and $2S+2$ for the compound system. Remember that S takes half-integer values for states with an odd number of electrons and is an integer if the number of electrons is even, which, of course, includes the close shell target case when $S=0$. Channels that only differ in the total spin are degenerate asymptotically but will show different behaviour in the short-range, inner region. The treatment of spin couplings can require careful treatment in the actual implementation of the problem (Tennyson 1997) but formal effects due to electron spin will not be discussed further here.

At large r_{N+1} the radial part of the continuum wavefunction, $F_{ij}(r_{N+1})$, behaves like a plane wave, which can be represented in terms of sine and cosines of kr_{N+1} where k is the wavenumber, which is related to the scattering energy, E, by,

$$k=\frac{\sqrt{2mE}}{\hbar}, \qquad (2)$$

where m is the mass of the particle, here, an electron that has mass $m_e=1$ in atomic units; $\hbar$ is Planck's constant divided by 2π. $\hbar$ is also equal to 1 in atomic units, which means that $E=\frac{k^2}{2}$ in atomic units (which for the energy are known as Hartree). Of course, it is also possible to use the complex exponential representation of a plane wave, $\exp\left(\pm ikr_{N+1}\right)$.

Since both the incoming and outgoing waves are plane waves, what characterizes an (elastic) scattering event for a single-channel problem is the phase shift, δ, between these waves, see figure 3. As can be seen from the figure, the phase shift corresponds to a change in the angle of the plane wave; phase shifts are generally given in radians. The phase shift captures the information on interactions that occur during the collision for a single-channel problem.

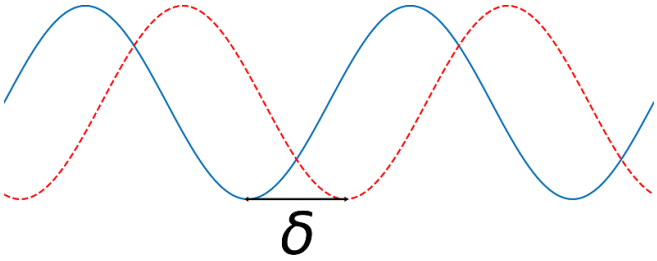

Figure 3. Schematic of two plane waves that differ by a phase shift of δ.

For a multi-channelled system, it is necessary to generalize the asymptotic plane wave expression to:

$$\begin{array}{lll} \text{Open channels} & F_{ij} \sim & \frac{1}{\sqrt{k_i}}\left(\sin\left(k_i r+\frac{1}{2}\ell_i\pi\right)\delta_{ij} \right. \\ & & \left. +\cos\left(k_i r+\frac{1}{2}\ell_i\pi\right)K_{ij}\right) \\ \text{Closed channels} & F_{ij} \sim & 0 \end{array} , \quad (3)$$

where open channels are ones where the states are energetically accessible at infinite separation, while closed channels cannot be accessed at this limit but may still have an important influence on the scattering process. Expression (3) is correct for a neutral target. If the target molecule is charged, there is an additional Coulomb phase to consider (Volkov *et al* 2009). For the multi-channel problem, one has to consider the coupling between channels, here between channels i and j. As a result of this coupling, the effect of scattering is represented by a **K** matrix, which is a real symmetric matrix of the number of open channels. Hazi (1979) showed that the equivalent of the phase shift for a multi-channel problem can be obtained by summing the eigenvalues obtained by diagonalizing the K-matrix:

$$\delta = \sum_i \arctan\left(K^D_{ii}\right), \quad (4)$$

yielding the eigenphase sums, or more commonly simply the eigenphase as a function of the scattering energy.

Analysis of eigenphases is an important tool in the theoretician locker as they contain a considerable amount of information on the scattering process. As discussed below, eigenphases are used to characterize resonances and can also be used to detect the presence of (extra) bound states (Levinson 1949). Attractive potentials give rise to positive eigenphases while the eigenphases are negative for repulsive interactions, while a zero eigenphase means that for that energy the target is effectively transparent, which leads to the presence of a Ramsauer minimum (Ramsauer 1921) in the cross-section. From a theoretical perspective, perhaps the most important (and least documented) reason for reading eigenphases is that they can provide an important diagnostic of problems with the calculation. Problematic calculations often yield physically plausible cross-sections but give eigenphases that contain tell-tale signs of issues with the calculations.

In principle, the **K** matrix contains all the known information about the collision process. In practice, two other (complex) matrices are often used to derive cross-sections and other key properties. They are the scattering (**S**) matrix:

$$\mathbf{S} = \frac{(\mathbf{I}+i\mathbf{K})}{(\mathbf{I}-i\mathbf{K})}, \quad (5)$$

and the transition (**T**)

$$\mathbf{T} = \mathbf{S}-\mathbf{I}, \quad (6)$$

where **I** is the unit or identity matrix with 1 along the diagonals and zero elsewhere. **S**-matrices are used to obtain the time-delay in the scattering process (Smith 1960), see below, and for multi-channel quantum defect theory analysis (Seaton 1983, Tennyson 1988) of problems. **S** and **T** matrices are square complex matrices of the total (open plus closed) number of channels.

Note that while the definitions of the **K** and **S** matrices given above are uniformly adopted, there are various definitions of the **T** matrix in use, which differ by no more than a phase factor. I favour the definition of equation (6) because of its simplicity.

3.3. Short range

At small electron-molecule distances it is necessary to generalize equation (1) to allow for detailed interaction with the target wavefunction. The standard form used for the $N+1$ electron system wavefunction in most treatments of low and intermediate energy scattering is:

$$\begin{aligned} \Psi_k^{(N+1)} = \mathcal{A}\sum_{ij} a_{ijk}\phi_i^N\left(\underline{r}_1\ldots\underline{r}_N\right)F_{ij}\left(r_{N+1}\right)Y_{\ell m}\left(\hat{r}_{N+1}\right) \\ +\sum_i b_{ik}\chi_i^{N+1}\left(\underline{r}_1\ldots\underline{r}_{N+1}\right), \end{aligned} \quad (7)$$

where the antisymmetrization operator, $\mathcal{A}$, is introduced to ensure that the $N+1$ electrons obey the Pauli principle, meaning that the wavefunction is antisymmetric with respect to the interchange of any two electrons. The second, extra term in equation (7) is a short-range ('L^2') term, which allows for the detailed interaction of the scattering electron with the target, for example by allowing it to occupy low-lying, unoccupied orbitals associated with the target.

3.4. Resonances

Resonances play a very important role in electron–molecule scattering. Resonances are quasi-bound states that lie in the continuum. That is, the electron hits the target and sticks for a finite amount of time before some process, most commonly (radiationless) autoionization or capture of the electrons, which leads to break-up of the resonance state. Since resonances have a finite lifetime, the uncertainty principle dictates that they do not possess an exact energy. Resonances are therefore generally characterized by both a position (E_r), which is generally given as an energy relative to the energy of the target ground state, and a width (Γ) that is inversely proportional to the life-time.

In terms of the eigenphase, the resonance is characterized by an increase in the eigenphase by π. Figure 4 compares eigenphases computed with two models for electron scattering from LiH; the simple SE model gives smooth eigenphases with no apparent resonance feature, while the more sophisticated five-state CC model shows a clear resonance feature at about 3.5 eV. Resonances usually appear as peaks in the cross-section; figure 5 gives the most notable example where for electron collisions with molecular nitrogen in the region of the low-lying resonance at 2.4 eV the total cross-section is increased by a factor of about three and is completely dominated by the rather broad resonance structure.

Resonances facilitate certain processes. In the case of the N_2 example considered in figure 5 the dominant process in the resonance region is vibrational excitation; dissociative recombination (DR) and dissociative electron attachment (DEA) are important processes, which only occur via resonance. These and other collision processes are considered below in section 5.

While resonances are often visible in cross-sections, analyzing the calculated cross-sections does not usually provide the most reliable method of obtaining (E_r,Γ) values that characterize a resonance. Instead, there are two main methods of obtaining resonance parameters from scattering calculations. The first is by fitting the jump of π in the eigenphase, see figure 4, to the form given by Breit and Wigner (1936), for which there are automated procedures for detecting and fitting (Tennyson and Noble 1985) resonances. The second method uses the semi-classical idea of a time delay in the scattering process caused by the temporary formation of a resonance; the S-matrix can be used to construct a time-delay matrix (Smith 1960) whose eigenvalues represent the length of the time-delay in the scattering process in each channel. Long time delays can be associated with a resonance. Again, there are also available procedures for detecting and fitting long time delays (Little *et al* 2017).

There are three distinct physical mechanisms for forming a resonance in electron–molecule collisions, which give resonances, generally known as shape, Feshbach and nuclear excited resonances.

Shape resonances generally occur at low scattering energies and are short-lived (broad). There are two explanations for the mechanism which, while seemingly rather different, are actually consistent with each other. A shape resonance can occur when the scattering electrons gets temporarily trapped behind the centrifugal barrier due to electron angular momentum. In atomic units, this barrier adds a term as follows:

$$\frac{\ell(\ell+1)}{r^2}, \tag{8}$$

to the potential, which means that shape resonance should not occur for s-wave scattering for which $\ell = 0$. Alternatively, shape resonances can be characterized by the scattering electrons entering a low-lying unoccupied target orbital. For example, for H_2 there is a very broad, low-lying shape resonance. This $^2\Sigma_u^+$ symmetry quasi-bound state of H_2^- can be

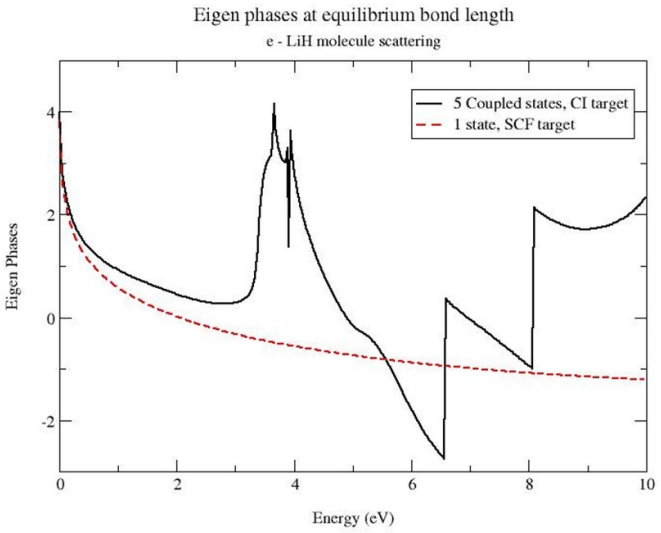

Figure 4. Eigenphase sums two models of electron scattering from LiH due to Antony *et al* (2004): red dashed line is a static exchange (SE) calculation while the solid black line is a five-state CC expansion calculation. Note that the discontinuities in the CC calculation at high energies are caused by adding factors of π to the eigenphase to restrict the range of the graph; eigenphases are arbitrary to factors of π.

represented by the configuration $1\sigma_g^2 1\sigma_u^1$, i.e. the scattering electrons enter the $1\sigma_u$ lowest unoccupied molecular orbital. Asymptotically, this shape resonance goes to the H+H$^-$ dissociation limit. Given that H$^-$ is bound (by about 0.75 eV), this means that at some point the resonance curve crosses that of the H_2 ground state and becomes a truly bound state. For internuclear separations beyond this point $\Gamma = 0$, see the middle panel of figure 10 below for an example of this behaviour.

An important characteristic of a shape resonance is that the state of the target is essentially unchanged. Conversely, Feshbach resonances always involve excitation of the target with the electrons trapped in the electronically excited state, often referred to as the parent state. Thus, for example, the lowest Feshbach resonance in H_2 is the $^2\Sigma_g^+$ symmetry state characterized by the $1\sigma_g^1 1\sigma_u^2$ configuration. In this example, the b $^3\Sigma_u^+$ and B $^1\Sigma_u^+$ both act as parent states. Feshbach resonances are usually much narrower (long-lived) than shape resonances and found at higher energies. Indeed, it appears to be common for there to be many Feshbach resonances in the region approaching the ionization threshold, see Celiberto *et al* (2012) for a discussion of these in H_2; for most molecules, resonances in this higher energy region remain uncharacterized. Collisions with molecular ions lead to an infinite series of Feshbach resonances associated with each electronically excited state of the ion. Feshbach resonances can occur for any ℓ value and, indeed, in the case of ionic targets occur for all ℓ values.

Nuclear-excited or nuclear-excited Feshbach resonances are the third, less common, class of resonances, which, unlike shape or Feshbach resonances, do not occur in atoms. These

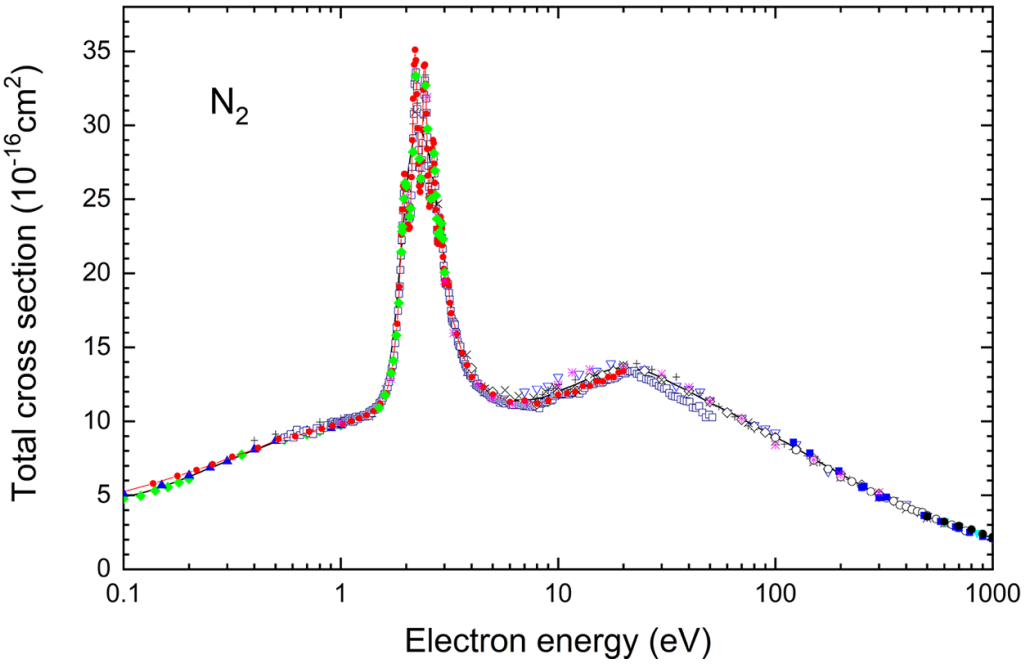

Figure 5. Total cross-sections for electron collisions with molecular nitrogen adapted from Song *et al* (2023), where details of the various experimental measurements represented by the different symbols are given.

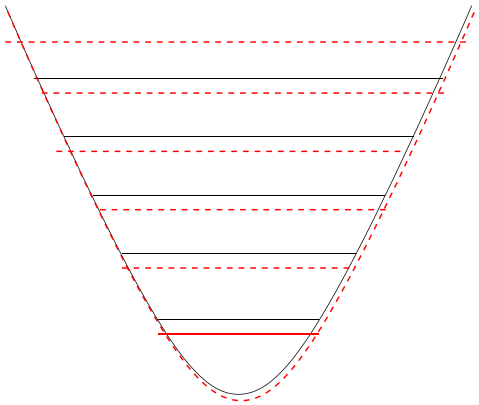

Figure 6. Diagram depicting the states involved in nuclear-excited Feshbach resonance. Solid black curve denotes the potential of the diatomic target potential with solid black horizontal lines denoting target vibrational states. Dashed red curve denotes the (weakly bound) potential curve of an anionic state of the target with horizontal lines, red denoting anionic vibrational state. Lowest ($v = 0$) anionic state represented by a solid red line is bound; the higher anionic vibrational states are all resonances that can decay via autoionization to a lower vibrational state of the target.

resonances are found in molecular targets that support very weakly bound anionic states of the target, see figure 6. Vibrationally excited states of this bound state can lie in the continuum and leads to the formation of very narrow resonances in these excited nuclear-motion states. Nuclear-xcited resonances have been well studied in the context of the complex resonance structures observed near the vibrational excitation thresholds in hydrogen halides, see Thümmel *et al* (1992) for example.

Given that resonances appear to have many of the characteristics of bound electronic states and the availability of many quantum chemistry codes, some authors have been tempted to use the results obtained directly from the quantum chemistry codes to predict resonance positions. As discussed by Stibbe and Tennyson (1999), this is extremely dangerous and can easily lead to fallacious results. Figure 7 gives a comparison between a quantum chemistry calculation of resonance positions (Mebel *et al* 1998) of H_2 with the results of a full scattering calculation (Stibbe and Tennyson 1998a).

While I strongly discourage the blind use of quantum chemistry procedures to characterize resonances, it is possible to adapt so-called '$L^{2\prime}$ methods for this purpose. Techniques for doing this have been developed by Sommerfeld and coworkers, see Davis and Sommerfeld (2021), Falcetta *et al* (2023) and references therein.

4. Methods and models

Solving a theoretical problem like electron–molecule scattering requires first building a suitable model and then using an appropriate method to solve for that model. Over an extended time, tests between methods known to give reliable solutions for a given model have demonstrated that results are not strongly dependent on the choice of methodology, examples include an early comparative study on electron—H_2 electronic excitation (Baluja *et al* 1985, Lima *et al* 1985, Schneider and Collins 1985), electron collisions with the molecular ion H_3^+ (Orel and Kulander 1993, Faure and Tennyson 2002), and indeed the CCC—RMPS comparison by Meltzer *et al* (2020) discussed above and illustrated in figure 2. Conversely, the

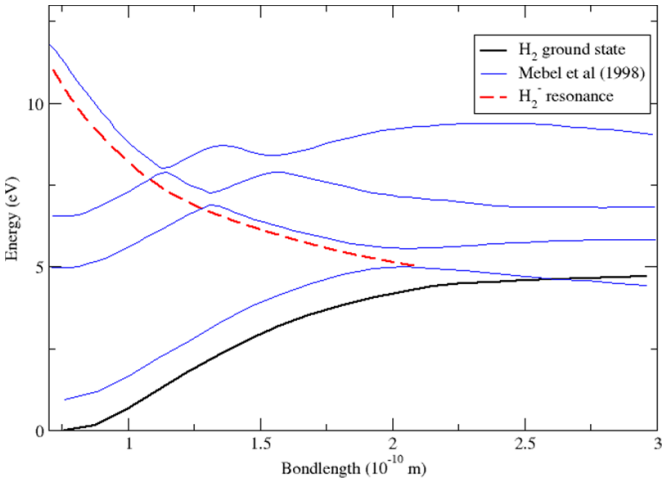

Figure 7. H_2^- 'Resonance' positions, in eV, with $^2\Sigma_g^+$ total symmetry as a function of internuclear separation, R in Å. Solid lines: results of a bound state in the continuum calculations performed using quantum chemistry code Gaussian by Mebel *et al* (1998); dashed line position of the well-known $^2\Sigma_g^+$ H_2^- Feshbach resonance calculated using a coupled-channel R-matrix calculation (Stibbe and Tennyson 1998a). Analysis from Stibbe and Tennyson(1999).

use of improved models can and often does lead to significantly different results. This was illustrated by Gorfinkiel and Tennyson (2004) for the electron—H_3^+ problem where the use of an RMPS model led to the inclusion of polarization effects not fully treated in the earlier calculations cited above.

Currently, there are three *ab initio* methodologies in widespread use for solving low-energy electron–molecule collision problems. These are the R-matrix method (Tennyson 2010, Burke 2011), Schwinger multi-channel variational method (Takatsuka and McKoy 1981, da Costa *et al* 2015) and Kohn variational method (Rescigno *et al* 1995). While each of these methods has its particular strengths and weaknesses, I will only consider the R-matrix method in any detail below, not just because this is the method I use, but also because it is currently by far the most widely used method.

It is common practice to refer to particular calculations by the method such as an 'R-matrix' or a 'Kohn' or a 'Schwinger' calculation. In my view, this practice is unhelpful as the major determinant of the result is not the method but the model. I note that quantum chemists refer to calculations by the model used (HF, density functional theory, multi-reference configuration interaction, etc) rather than the method used to solve it (Molpro, Gaussian, etc). In my view, the electron–molecule collision community should follow this practice. Below, I consider some of the characteristics of the models generally in use today, namely the SE model, static exchange plus polarization (SEP) model and CC model. I will also consider the intermediate energy procedures CCC and RMPS, which blur the distinction between methods and models since the model used in each of these cases is method specific. First, however, I give some details of the R-matrix method.

4.1. The R-matrix method

The R-matrix method was originally proposed by Wigner and Eisenbud (1947) as a phenomenological method for treating scattering problems in nuclear physics where the details of the short-range interactions are unknown. Wigner and Eisenbud (1947) simply parameterized the inner region interactions on a spherical boundary and solved the resulting outer region problem. Phillip Burke was the father of what has come to be known as the calculable R-matrix method (Bartschat *et al* 2020). Burke realized that for atomic, and subsequently molecular, problems it is indeed possible to compute the interactions in the inner region and then use these to parameterize the problem on the boundary *ab initio*. Burke (2011) remains the authoritative book on the subject.

Thus, the basis of the R-matrix method is the division of space into two regions: an inner region where a full treatment of exchange and correlation (polarization) is required and an outer region where a simplified, potential scattering problem can be solved. The major advantage of this approach is that while the relatively simple outer-region problem has to be solved at each scattering energy of interest, the computationally more challenging inner-region problem needs only to be solved once to provide these solutions as a function of scattering energy. In the R-matrix method, the inner region is described by a sphere that must be sufficiently large to enclose the charge distribution (or wavefunction) of the target species.

Since the inner-region problem is solved independent of scattering energy, it has strong similarities with the standard electronic-structure problem solved for molecules by quantum chemists. A detailed, although slightly dated, review of the molecular R-matrix method was given by Tennyson (2010) to which the reader interested in formalism and other technical details is referred.

If one thinks of the inner region as an adaptation of a quantum chemistry electronic-structure problem, then there are a number of technical issues that need to be overcome: (i) one needs appropriate basis functions to represent the continuum electron (function F_{ij} in equation (7)); (ii) integrals must be performed over the finite region enclosed by the R-matrix sphere, something that technically is easier than it might at first appear (Nestmann *et al* 1991, Morgan *et al* 1997); (iii) special measures are required to keep additional continuum basis functions (or orbitals) orthonormal to the target orbitals; (iv) significantly more high ℓ functions are needed to represent the continuum than is usual in the standard electronic problem (surprisingly, at least to me, this causes severe problems with most standard quantum chemistry codes); (v) finally, since the essence of the method is to compute differences between the N-electron target problem and $(N+1)$-electron scattering, the selection of target and scattering models as implied by the choice of electron configurations must be balanced in a way not usually considered by the electron configuration generators available in standard quantum chemistry codes. This means that the various UK R-matrix codes discussed below still rely on adaptations of a very

flexible configuration generator developed half a century ago by Yoshimine (1973), albeit as the driver of a highly efficient means of generating the full scattering Hamiltonian (Tennyson 1996a, Al-Refaie and Tennyson 2017). In this formulation, the inner-region problem becomes one of diagonalizing the inner region Hamiltonian matrix to determine the R-matrix eigenenergies and corresponding wavefunctions is in the form of values for coefficients $\underline{a}$ and $\underline{b}$ of equation (7). Note that unlike standard bound state problems, all solutions of the inner-region problem (or a significant proportion of all the solutions (Tennyson 2004)) are required in order to construct the R-matrix at the boundary with the outer region.

The treatment of electron collisions from polyatomic molecules has generally used Gaussian-type orbitals (GTOs) to represent the continuum (Nestmann and Peyerimhoff 1990, Faure *et al* 2002), although more recently Mašín and Gorfinkiel (2014) also implemented B-spline basis functions as an alternative means of representing the continuum. B-splines have the advantage of allowing much larger inner regions to be used when necessary (Meltzer *et al* 2020). The current version of the UK molecular R-matrix code, UKRmol+ (Mašín *et al* 2020), offers GTOs, B-splines and a mixture of both as continuum basis functions.

Having solved the (scattering energy-independent) inner-region problem, the energy-dependent R-matrix is constructed on the boundary using the eigenenergies determined for the inner-region problem and the corresponding amplitudes of the continuum functions on the boundary. These R-matrices are then propagated (Morgan 1984) before use to some large distance, typically between 100 and 250 a_0. At this point, the K-matrix at each energy is determined using an asymptotic expansion due to Gailitis (1976), see Burke and Noble (1995) for more details of these procedures. Note that in the outer region the R-matrix is a matrix that relates the radial function $F_{ij}(\underline{r}_{N+1})$ to its derivative at a given $\underline{r}_{N+1}$. This means that, in common with other log-derivative propagators (Friedman and Jamieson 1995), propagation of the R-matrix is numerically much more stable than treating the wavefunction directly in the outer region, as wavefunctions of exponentially decaying closed channel solutions can become exponentially increasing due to numerical noise. However, the use of R-matrix propagation means that standard R-matrix calculations do not obtain outer-region wavefunctions.

The UKRmol+ codes, which have also been extended to treat standard photoionization (Brambila *et al* 2015), multi-photon ionization (Benda and Mašín 2021) and time-dependence in strong laser fields (Benda *et al* 2020, Brown *et al* 2020), are freely available via Zenodo repositories for the inner (Mašín *et al* 2019) and the outer (UK R-matrix community 2021) repositories. There is also a commercially available expert system called QECs (Quantemol electron collisions) (Cooper *et al* 2019) built on the use of UKRmol+ and the electronic structure code Molpro (Werner *et al* 2020). QEC facilitates the calculation of electron collision processes by non-experts.

4.2. Models: static exchange

In the SE approximation, the target is represented by the ground state of the molecule as a single-configuration wavefunction generally generated using an HF calculation. In this model, the general form of equation (7) reduces to:

$$\Psi_k^{(N+1)} = \mathcal{A}\sum_j a_{jk}\phi^N(\underline{r}_1\ldots\underline{r}_N)F_j(r_{N+1})Y_{\ell m}(\hat{r}_{N+1}) + \sum_i b_{ik}\chi_i^{N+1}(\underline{r}_1\ldots\underline{r}_{N+1}), \quad (9)$$

where sum over target states has been reduced to a single term and the so-called 'L^2' second term in the sum has a particularly simple form where only the scattering electrons are allowed to occupy an empty ('virtual') target orbital retained in the model. These configurations are important since they allow for high ℓ behaviour in the vicinity of the target. Usually, SE calculations do not require many virtual orbitals to reach convergence, but care must be taken to include all the virtual orbitals that provide the home for resonances (Trevisan *et al* 2006).

As the name of the model implies, the SE approximation captures the static interactions between the scattering electrons and the target such as electron–dipole interactions and the exchange interactions caused by the overlap of the electron with the target wavefunction. The model makes no allowance for correlation between the scattering electrons and the target electrons, or equivalently, polarization of the target by the incoming electrons.

The SE model is a well-defined model for which all codes should and generally do give the same result. It captures the long-range physics of the problem and can, in principle, work at all collision energies. An SE calculation recovers shape resonances, usually at too high an energy due to the neglect of polarization effects, but does not give Feshbach resonances. Whether a resonance is present in an SE calculation can therefore be used to indicate whether it is shape or Feshbach in nature.

4.3. Models: static exchange plus polarizability

The SEP model is also based on scattering from a one-state HF target wavefunction. The equation for the SEP wavefunction therefore has the same form as that for the SE approximation, equation (9). The difference between the SE and SEP approximations comes from the treatment of the 'L^2' second term. The SEP approximation includes an extra configuration type, which involves the excitation of a single target electron in a target virtual orbital combined with the scattering electron also entering a virtual orbital. This two-particle, one-hole (2p,1h) configuration model targets polarization effects or, alternatively, allows for correlation between the scattering electrons and the target electrons. Typically, SEP calculations require the use of larger sets of virtual orbitals than SE calculations (Fujimoto *et al* 2012). However, even with large sets of virtual orbitals, SE and SEP calculations are computationally cheap.

The SEP model provides a very simple and efficient method of representing shape resonances. It can also capture Feshbach

resonances but, in the absence of parent electronically excited states in the calculation, Feshbach resonances are not always reliably represented. The inclusion of the (2p,1h) configurations limits the energy range of the SEP model to energies below the first electronically excited state of the target; above this energy the (2p,1h) configurations give rise to a series of artificial resonances known as pseudo-resonances.

Practical implementations of the SEP method can differ slightly between codes, leading to subtly different results. However, more serious is the problem that the method can become unbalanced. Essentially, one is using an uncorrelated, HF target and then adding a highly correlated electron meaning that the treatment of $(N+1)$ is better than, i.e. not balanced with, the treatment of the N electron system. In practice, scientists have found that careful use of the SEP approximation can give excellent results for important low-lying shape resonances, but there is probably an element of pragmatism in how these calculations are performed.

4.4. Models: the close-coupling approximation

The SE and SEP models do not allow for electronic excitation; to include this one has to use a method that couples together target electronic states such as the CC approximation. The form of the (inner region) wavefunction given by equation (7) including a sum over target states represents the CC approximation. Although it is possible to use HF wavefunctions in the CC approximation (Falkowski *et al* 2023), this is not generally done since the HF approximation usually gives a poor representation of electronically excited states. The most common form of the target wavefunction used is generated using a complete active space configuration interaction (CAS-CI) procedure where, typically, the valence electrons are allowed to move freely within all valence orbitals and the core electrons are frozen in their original Hartree–Fock (or CAS-SCF) orbital. Within this model, the scattering electrons are also allowed to enter this CAS space giving $(N+1)$ electrons; the representation of polarization effects can be further improved by adding extra target virtual orbitals to the model (Tennyson 1996b).

CC calculations capture short-range polarization effects, albeit less efficiently than in an SEP calculation, and also allow for these effects in the outer region due to dipole coupling between the states (Jones and Tennyson 2010). This method therefore does a more thorough treatment of channel coupling effects.

The CC method captures both shape and Feshbach resonances. While shape resonances may not be as well treated as in the SEP approximation, the explicit inclusion of the parent state(s) into the calculation leads to a very accurate representation of Feshbach resonances, see Stibbe and Tennyson (1997) for example. The energy range is extended compared to the SEP model and increases to the energy of the first target state omitted from the CC expansion. In practical terms, given the infinite number of electronic states below the ionization threshold, this means that CC calculations can only hope to reliably cover energies below the threshold for ionization.

4.5. Models: extension to intermediate energies

The key to extending CC methodologies above the ionization threshold and into the intermediate energy regime is constructing some (pseudo)-complete representations of the electronic states of the target up to and even beyond the ionization threshold. A key element in achieving this is the realization that highly excited target states become increasingly diffuse. However, if one is scattering from a ground (or low-lying) state it is only necessary to have some sort of representation of these highly excited states in the fairly compact spatial region occupied by these low-lying states.

The gold standard method for treating the intermediate energy regime is the CCC method. Originally developed for atoms by Bray and Stelbovics (1992), it was subsequently extended to molecules, see the tutorial review by Zammit *et al* (2017). The basic idea of the CCC method is to provide the complete representation of the target by a set of (pseudo)states generated by diagonalizing its electronic Hamiltonian in a basis of Sturmian (Laguerre) functions. The CCC method has been shown to be very powerful for treating simple targets, such as H_2, for which comprehensive electron collision data sets are now available over an extended energy range (Scarlett *et al* 2021a, 2021b, 2022, 2023). However, thus far, its use has been restricted to targets with few (active) electrons.

A similar RMPS method was developed to treat intermediate energy electron–atom collisions (Bartschat 1998). In common with the CCC approach, the RMPS generates a quasi-complete set of target (pseudo)states in the R-matrix inner region. This idea was extended to molecules (Gorfinkiel and Tennyson 2004, 2005). The RMPS method can treat systems with many active electrons and has been used for some novel calculations (Halmová and Tennyson 2008, Zhang *et al* 2011), but its use has so far been restricted by the fact that the method is very computationally demanding.

The CCC and RMPS methods capture all polarizations and state couplings, and give good results over a greatly extended energy range, for example, the CCC H_2 studies cited above extend up to 1000 eV (Scarlett *et al* 2023). Of course, the methods give a good representation of both shape and polarization effects, but the RMPS method also gives pseudo-resonances at higher energies whose effects are usually just smoothed over. An advantage of these methodologies is that the computation of the target polarizability can be used as a proxy to gauge the convergence of polarization effects in the whole calculation (Jones and Tennyson 2010).

4.6. Uncertainties

Since computed cross-sections and rates are increasingly being used in models of key problems in plasma technology, fusion science, etc, it has become increasingly important for the uncertainties inherent in the computed data to be quantified. However, theorists are notoriously unwilling to provide uncertainties with their calculated data. Uncertainty quantification in electron collision problems was considered by Chung *et al* (2016). The problem has a number of key characteristics:

(i) the problem being solved is generally well characterized in terms of the equations of quantum mechanics, which are not easily solved; (2) the methods used to solve the scattering problem are usually numerically robust so the results suffer little from numerical noise; (3) the choice of model and related issues such as basis-set size and configuration list are the major causes of uncertainty; these uncertainties are systematic rather than statistical. It remains early days in the uncertainty quantification of electron–molecule collision calculations, but it will undoubtedly be something that is increasingly attempted in the future.

5. Processes

Electron collisions with molecules can result in a variety of outcomes, as summarized for collision energies up to the ionization threshold of their target in table 1. Note that a number of these processes, such as vibrational excitation, dissociative attachment and DR require treatment of nuclear motion alongside the electron impact. However, there is no completely general, practicable theory that would allow a full simultaneous treatment of the electron and nuclear dynamics in a single calculation. This means that in practice it is not possible to treat all processes in a single calculation. Therefore, I will consider the treatments of each process in turn, in some cases in pairs when similar treatments are required for both processes.

5.1. Elastic and rotational excitation cross-sections

Elastic scattering involves no net energy exchange between the scattering electron and the target molecule. It may therefore seem that the process is trivial, but this is not true since elastic scattering can involve transfer of momentum between the electron and the target, and a change in direction of the incoming electron, which can be significant if, for example, the original electron flux is in the form of a collimated beam such as in a lightning bolt. To understand both these processes it is necessary to consider the differential cross-section (DCS).

The DCS measures the cross-section as a function of the deflection of the electron from its original trajectory, as denoted by angle θ in figure 8. When $\theta = 0$, the electron carries straight on even if there has been a collision and no momentum is transferred; this is called forward scattering. Conversely, if $\theta = 180^o$, the electron is backward scattered to where it originally came from. Backward scattering involves a significant momentum transfer. Thus, the total cross-section, $\sigma(E)$, is derived from the DCS by:

$$\sigma(E) = 2\pi \int_0^{\pi} \frac{\mathrm{d}\sigma}{\mathrm{d}\theta} \sin\theta \mathrm{d}\theta, \tag{10}$$

where the factor of 2π comes from integration over the other polar angle ϕ for which the scattering event is symmetric for a freely rotating gas-phase molecule. The momentum transfer cross-section, $\sigma_M(E)$, obeys a similar formula but with an extra angular weighting of zero for forward scattering and two for backward scattering:

$$\sigma_M(E) = 2\pi \int_0^{\pi} \frac{\mathrm{d}\sigma}{\mathrm{d}\theta} (1 - \cos\theta) \sin\theta \mathrm{d}\theta. \tag{11}$$

Table 1. Possible processes resulting from an electron–molecule collision in approximate order of increasing threshold energy: AB denotes an arbitrary molecule.

Process name	Process		
Elastic scattering	$AB + e$	$\rightarrow$	$AB + e$
Rotational excitation	$AB(J'') + e$	$\rightarrow$	$AB(J') + e$
Vibrational excitation	$AB(v'') + e$	$\rightarrow$	$AB(v') + e$
Dissociative recombination	$AB^+ + e$	$\rightarrow$	$A + B$
Dissociative electron attachment	$AB + e$	$\rightarrow$	$A + B^-$
Electronic excitation	$AB + e$	$\rightarrow$	$AB^* + e$
Impact dissociation	$AB + e$	$\rightarrow$	$A + B + e$
Impact ionization (e,2e)	$AB + e$	$\rightarrow$	$AB^+ + e + e$

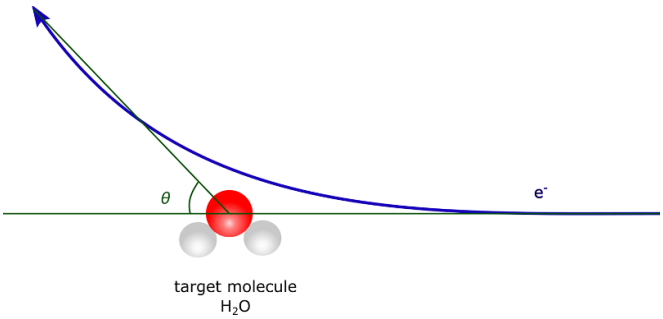

Figure 8. DCS, $\frac{\mathrm{d}\sigma(E)}{\mathrm{d}\theta}$, is the cross-section for the electron with energy E to be deflected by angle θ.

Figure 9 shows the DCS of water. Water has a permanent dipole; note that its DCS is very strongly forward peaked. The elastic cross-section can be measured by sending a beam of electrons across a gas sample and either measuring the attenuation of the beam, which gives the cross-section using the Beer–Lambert law or by collecting the scattered electrons as a function of θ to give the DCS, which can then be integrated to give the total cross-section. Either way, there is a problem doing this for systems with a permanent dipole.

Systems with permanent dipoles scatter electrons strongly in the forward direction. However, in practical terms, it is very difficult to distinguish an electron that has been scattered in the forward direction from an electron that is simply an unscattered part of the original beam. Typically, experimental measurement of the DCS for angles less than about 15^o is not possible, for an exception see Kadokura *et al* (2019). If most of the flux gets scattered to very small angles, as is the case for water and other dipolar systems, then the measurements will strongly underestimate the total cross-section (Zhang *et al* 2009). This means that experimental cross-sections for such systems are strongly underestimated unless some sort of (theoretical) correction is made to allow for low-angle scattering. Conversely, the Born approximation captures this behaviour, which is associated with the rather easy scattering of high ℓ partial waves. The contribution to the cross-section by partial waves with high ℓ that do not enter the inner region is analytic

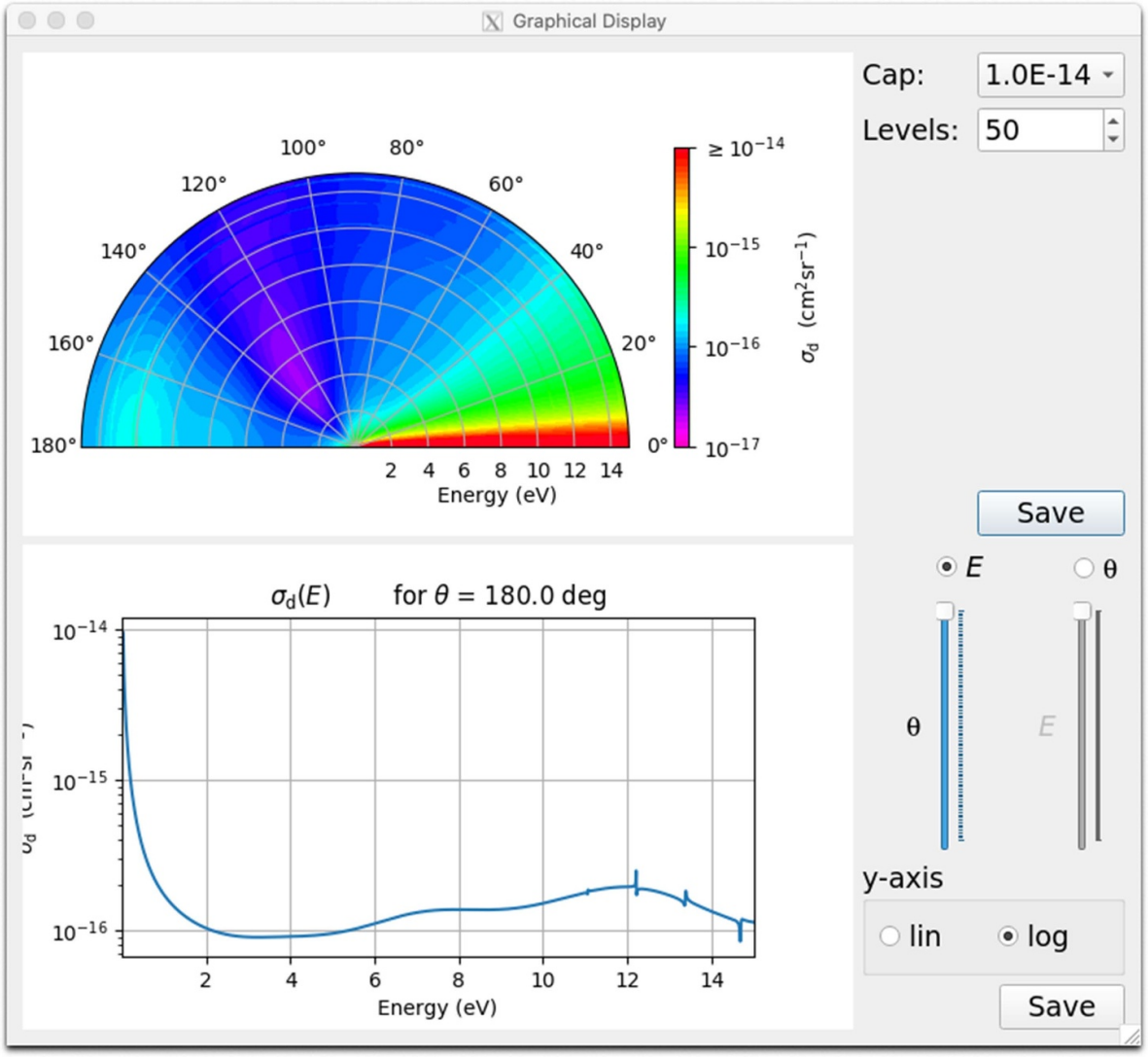

Figure 9. Example of the DCS of electrons with water calculated using the QEC expert system. Note that the DCS for this dipolar molecule is very heavily forward peaked.

(Padial *et al* 1981). This means that adjusting calculations for this behaviour is easy (Norcross and Padial 1982). Total elastic cross-sections for electron collisions with polar molecules are more reliably calculated than measured!

There is another issue with the measurements of the so-called elastic cross-sections. The spacing between rotational levels in molecules is so small that it requires very careful experiments to identify electron impact rotational excitation. Nearly all measurements of elastic cross-sections are not sensitive to changes in the rotational state of the molecule being studied. This means that instead of measuring the truly elastic cross-section corresponding to the initial and final rotational state being unchanged ($J' = J''$), what is usually being measured is the cross-section summed over all possible final rotational states (J's). Again, theoretically, it is relatively easy to compute the rotational excitation cross-section (Sanna and Gianturco 1998). These calculations are generally performed for a single fixed geometry of the target, which is appropriate for the generally assumed rigid rotor approximation.

Electron–water (rotationally averaged) elastic cross-sections and rotational excitations have been computed (Faure *et al* 2004a, 2004b) and compared with rotationally-resolved experiments (Jung *et al* 1982). While the theory can reproduce the experiment, there is not enough information in the experiment to resolve the individual cross-sections. A similar situation occurs with electron collisions with molecular ions (Shafir *et al* 2009, Kalosi *et al* 2022).

Rotational excitation of molecular ions is particularly important for astrophysics since for ions with a permanent dipole moment these cross-sections are very large. In photon-dominated regions of the interstellar medium the electron (number) density can increase to about 10^{-4} times that of H_2, which is assumed to be the major collision partner. H_2 is not very efficient at exciting rotational states and as a result, the rate of collisional excitation by electrons is typically $>10^5$ larger, meaning that even for relatively low electron density electrons become the major means of exciting the molecules. These very low-pressure environments are not thermalized,

meaning that radiative lifetimes are typically much shorter than the mean time between collisions; this means that each electron collision results in emission of a photon. Therefore, to obtain concentrations (or column densities) of the radiating species, it is necessary to know the collision rates.

The simplest theoretical model of electron impact rotational excitation of dipolar molecular ions is the dipole Coulomb–Born approximation, which gives an analytic formula for the cross-section (Crawford *et al* 1967) based on the assumption that only (long-range) dipole interactions need to be considered. Within this model, only $\Delta J = 1$ excitations are possible, which means that only $J = 1 - 0$ emissions should be observed. However, observations suggest that for some key species emissions from higher rotational states are strong, up to $J'' = 7$ in the case of the important ion CH^+ (Cernicharo *et al* 1997) for example. This has led to the examination of the theory of electron impact rotational excitation of molecular ions (Faure and Tennyson 2001), which broadly speaking shows that for molecules with large permanent dipole moments (bigger than about 2 Debye) the Coulomb–Born model is satisfactory and the $\Delta J = 1$ collisional excitation is dominant. However, for ions with smaller dipole moments, it is necessary to also consider short-range interactions that provide the mechanism for changes with $\Delta J \geqslant 2$. Calculations show that in the small dipole case $\Delta J = 2$ excitations are always important and can even be bigger than $\Delta J = 1$ (Rabadán *et al* 1998); and that excitations with $\Delta J > 2$ are usually small, but $\Delta J = 3$ excitation is sometimes significant (Faure and Tennyson 2001). It should be noted that for ions the dipole moment is isotope dependent, most notably H_2^+ does not have one but HD^+ does have a permanent dipole moment, which means that the collisional rotational excitation rates show strong isotope dependence. It has been suggested that the study of emission from interstellar molecular ions provides the most promising means of determining the local electron density (Jimenez-Serra *et al* 2006).

5.2. Vibrational excitation

Consideration of vibrational excitation as well as DEA/DR requires some consideration of nuclear motion. Given that treatments of nuclear motion are generally performed within the Born–Oppenheimer approximation, which gives rise to a separation between the (slow) motion of the nuclei and (fast) motion of the electrons, this leads directly to the need to consider two distinct cases. Case 1 is where the nuclear motion is considered to take place in the potential energy curves of the N-electron target and the electron simply has a short-lived interaction with the system; this is the basis for treating the direct vibrational excitation mechanism. In case 2, the electron and the target form a compound system, a resonance, and the nuclear motion occurs on potential curves given by this $N + 1$ electron system (see Stibbe and Tennyson 1997 as a good example of this). This is the basis for resonant vibrational excitation.

Considering the direct mechanism first, this process can occur at all energies above the threshold for vibrational excitation. This is largely driven by changes in the dipole moment, such as photon absorption, and is therefore dominated by single jumps in the vibrational state, $\Delta v = 1$. Compared to the resonance-enhanced vibrational excitations, the cross-sections are usually fairly small. A simplified treatment of direct vibrational excitation has recently been developed by Ayouz *et al* (2021) and is available as part of the QEC expert system.

Conversely, the resonance mechanism only occurs at specific energies where there is a resonance, see figure 10. In this mechanism, the electron is temporarily trapped in the resonance and evolves on the potential curve of the compound $N + 1$ electron system. This curve is complex due to the width (finite lifetime) of the resonance. Decays, which occur by autoionization of the resonance, can then occur for a range of vibrational states. Indeed, this mechanism can lead to very high vibrational states being excited; excitations with $\Delta v = 17$ have been observed in N_2 (Allan 1985). As can be seen from the large peak in the electron–N_2 cross-section, see figure 5, in the region of the $^2\Pi_u$ symmetry resonance, which is almost entirely due to the vibrational excitation cross-section in this region, resonance-enhanced vibrational excitation can be very efficient. Codes have been developed to treat this process (Laporta *et al* 2012, 2014). Any treatment of resonance-enhanced vibrational excitation needs to also consider the dissociative attachment/recombination processes considered in the next subsection.

5.3. Dissociative electron attachment and dissociative recombination

DEA and DR both require resonance curves that are linked to the dissociation products. For DEA, these are often the same curves that are considered for vibrational excitation, although of course, they must lie high enough that the dissociation channel is open. DEA can therefore be treated using the same methodology as resonance-enhanced vibrational excitation, see Laporta *et al* (2020) for example. Fabrikant *et al* (2017) provide a thorough discussion of the DEA process.

The treatment of DR is altogether more complicated. This is because, as discussed, ions support many infinities of resonance curves. DR can occur through two mechanisms: direct and indirect, see figure 11. In the direct mechanism, the resonance curve leads directly to dissociation. This process, if available, is usually dominant and gives fairly smooth cross-sections as a function of energy. The indirect mechanism, first identified by Bardsley (1968), is a two-step process whereby the electron initially enters a (non-dissociative) Rydberg state of the system, which then crosses with a dissociative curve, which provides a route to dissociation; indirect cross-sections are highly structured. The direct mechanism is not always available (Sarpal *et al* 1994) but when it is, it usually provides the dominant mechanism for DR. In practical terms, and taking DR of N_2^+ as an example, calculations of DR rates require bound-state Rydberg curves of the neutral system (Little and Tennyson 2013), resonance curve and width (often referred to as couplings in DR calculations) (Little and Tennyson 2014)

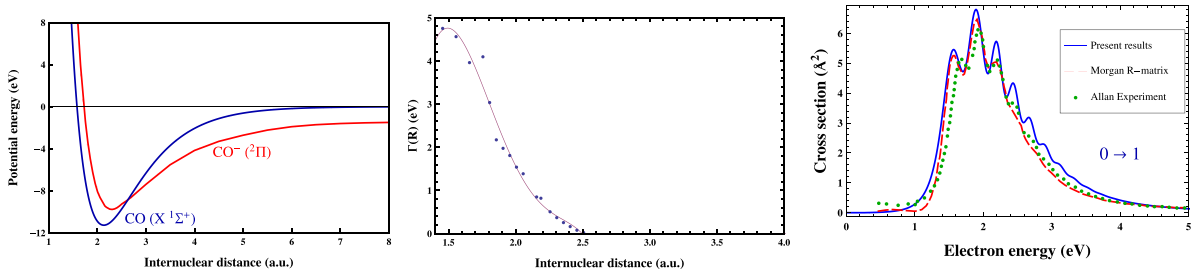

Figure 10. Calculated electron impact vibrational excitation of CO via its $^2\Pi$ shape resonance. Left: calculated potential energy and resonance curves; Middle: resonance width Γ as a function of C–O separation; Right: calculated cross-section for the $v = 1 - 0$ excitations compared to the measurements of Allan (2010) and the previous calculations of Morgan (1991); adapted from Laporta *et al* (2012).

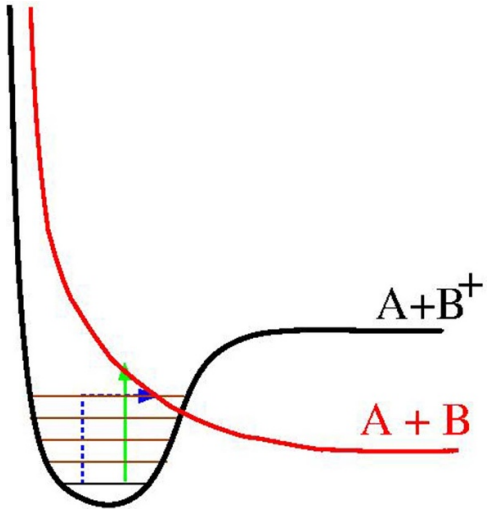

Figure 11. Schematic of the mechanisms for the dissociative recombination of molecular ion AB^+ from the ion ground state, as represented by the lowest (black) vibrational state on the black ion potential curve via the red dissociative resonance curve. Direct mechanism is represented by the vertical green arrow where the system enters directly into the dissociative resonance curve; the indirect mechanism represented by the blue dashed arrow involves excitation in to a (brown) nuclear excited resonance state from which it accesses the dissociative resonance.

and treatment of the nuclear motion on these curves (Little *et al* 2014, Abdoulanziz *et al* 2021). Multi-channel quantum defect theory, see the book by Jungen (1996), is often used as the final step since this theory allows the treatment of the entire Rydberg series. Wavepacket methods provide an alternative approach to treating this step, which is increasingly finding a role in the treatment of problems with more than two atoms (Larson *et al* 2012, dos Santos *et al* 2016). DR is thoroughly discussed in the book of Larsson and Orel (2008).

5.4. Electron impact electronic excitation and dissociation

The topics of electron impact electronic excitation and electron impact dissociation are grouped together because it is generally assumed that electron impact dissociation occurs via electronic excited states, so there is no need for a separate calculation. Within this assumption, the electron impact dissociation cross-section is simply taken as the sum of electronic excitation cross-sections lying above the dissociation limit. This assumption is based on the observation that direct dissociation, i.e. without electronic excitation, would correspond to a vibrational excitation process with a large Δv; while the resonant vibrational excitation process can also lead to dissociation (Laporta *et al* 2014), this is very much a minority process. More of the problem with the assumption of simply summing electronic excitation cross-sections is the treatment of near-threshold dissociation, which can depend strongly on the correct treatment of nuclear motion effects (Stibbe and Tennyson 1998b, Scarlett *et al* 2021c). In addition, when using electronic excitation and electron impact dissociation cross-sections in a (plasma) model, it is important to be careful how to use these cross-sections to avoid double counting.

Treatment of electron impact excitation has been the subject of many theoretical studies and I will only briefly discuss some of these issues. Clearly, this process can only be treated using a model that includes electronically excited states such as the ones that use a CC expansion. One also needs a reasonable representation of all the electronic states of interest both so that the energy thresholds appear close to the correct energies and the model generates physically appropriate target wavefunctions for use in the scattering calculations. Even for relatively simple molecular targets this can be very challenging, see the discussion by Brigg *et al* (2014) for methane. Methane is typical of many molecular targets in that it has very diffuse (Rydberg-like) excited states. Indeed, in the case of methane all the low-lying excited states are Rydberg-like. These states are difficult to treat both because, at least in R-matrix based procedures, they require the use of very large R-matrix spheres (Darby-Lewis *et al* 2017, Meltzer *et al* 2020) and because standard quantum chemistry procedures are not particularly good at representing Rydberg states.

When considering electronic excitation processes, it is common to consider whether the transition being considered obeys standard (photon) dipole selection rules. Spin changing transitions, such as excitation from a singlet ground state to a triplet excited, which usually provides the lowest electronic excitation process for a closed shell target, do not obey the dipole rule that $\Delta S = 0$ but are allowed in electronic collisions. In electron collisions, these transitions are

driven by short-range exchange interactions. This means that the cross-sections for these transitions peak at low energy (near threshold) and then drop to zero at high collision energies where exchange effects are generally unimportant.

Dipole-allowed transitions behave differently; their cross-sections often increase from threshold and remain significant at high collision energies. In partial wave treatments, it is usually necessary to add a Born correction to dipole-allowed transitions (Kaur *et al* 2008) to allow for high-lying partial waves to be neglected in the initial calculation in a fashion similar to that for elastic collisions discussed above. At higher energies, the dipole cross-sections for these transitions can be computed with the so-called BEf procedure where the f represents the electric dipole oscillator strength (Kim 2001). Similarly, the SCOP procedure provides information on the total inelastic cross-section such as the summed cross-section for all electronic excitations.

As mentioned above, nuclear motion can be important in the treatment of electronic excitation. Generally, where this has been considered, researchers have used the Franck–Condon approximation, which was originally developed for the treatment of transition intensities in photon-driven vibronic transitions but has become widely used for the simplified treatment of many molecular processes involving changes in electronic states. Use of the Franck–Condon approximation (Condon 1928), which attributes vibrational distributions on the basis of the squared overlap of the vibrational states to the electronic states of interest, is simple because it only requires the electron collision calculations to be performed in a single geometry, usually the equilibrium geometry of the electronic ground state. Treatments that use full averaging over geometry-dependent electronic excitation cross-sections have been performed (Darby-Lewis *et al* 2020).

Metastable (that is, long-lived) excited states are important in low-pressure plasmas where these states are not rapidly removed (thermalized) by collisions with other particles. These states can provide a stepping stone to other processes such as ionization. Electron collisions with these states are difficult to study experimentally but are conducive to calculations, see Su *et al* (2022) for example, although there are outstanding issues over the energy range for which current methods beyond the CCC approach can provide reliable treatments of these problems.

6. Data sources and summary

There is a large demand for electron collision cross-sections as input to models for a whole range of processes. This cannot be met by current experimental efforts, so there is increased use of theory to provide data for use in models of electron collision processes in plasmas and elsewhere. As a direct consequence of this, there has been a growing need for storing these results in a readily accessible and usable way. As a result, a number of databases have been developed to address this need. LXcat (Pitchford *et al* 2017) specializes in the provision of electron collision data from both theory and experiment for atoms and molecules; similarly, the Quantemol Database (QDB, Tennyson *et al* 2022) provides input for plasma chemistries and therefore provides both electron collision cross-sections and information on chemical reaction rates. BASECOL (Dubernet *et al* 2013, Dubernet *et al* 2024) provides atomic and molecular collision data for astrophysical studies and therefore includes the results of electron collision studies, mainly focussing on rotational excitation.

An alternative way of providing electron collision data sets is through systematic evaluation of all data, both experimental and theoretical, for a given molecular target or small group of targets (Karwasz *et al* 2023); a recent example is provided by the recent study of electron collision cross-sections for N_2 and N_2^+ (Song *et al* 2023). These compilations provide an important source of useful data, usually with associated uncertainties, but because they are usually driven by the availability of experimental studies, they are generally limited to stable species for which they have been well studied experimentally.

In response to the need for complete chemistry sets, there is the beginning of a trend whereby theoretical methods are used to generate electron collision cross-sections for a stable molecule and all its associated fragments. This process allows for some benchmarking of theoretical models against measurements on stable species. Examples of this type include studies of cross-sections for electron collisions with NH_3, NH_2 and NH (Snoeckx *et al* 2023) and with NF_3, NF_2 and NF (Hamilton *et al* 2017), which have formed the basis for models of plasmas that use NF_3 as a feedstock gas (Huang *et al* 2017, 2018).

7. Conclusion

Electron–molecule collisions are important in a whole variety of processes and therefore their continued study is important for understanding and modelling these processes. The volume and nature of data required for these studies has meant that theory rather than experiment has increasingly become the main source of such information. A few decades ago, theoretical methods for addressing the electron–molecule collision problem were undergoing what has been described as 'formalism wars', where different formulations of the problem were being proposed and tested. This period has now passed and there are a number of well-tested and robust methods available. Of course, there is always scope for further improvements in theoretical methods, including properly addressing issues such as uncertainty quantification.

Data availability statement

No new data were created or analyzed in this study.

Acknowledgments

I thank Greg Armstrong for helpful comments on the manuscript, and Charles Bowesman, Vincent Graves, Mi-Young Song and Armando Perri for help with the figures. I also thank the many people I have worked with on electron–molecule scattering problems and particularly those whose work I have used in this article. The tutorial is based on a Tutorial Lecture

given by me in Ottawa as prelude to the ICPEAC 2023 conference; I thank the organisers for inviting me to give this talk. I also thank STFC for award ST/R005133/1 which supported the development of the QEC expert system.

ORCID iD

Jonathan Tennyson https://orcid.org/0000-0002-4994-5238

References

Abdoulanziz A, Argentin C, Laporta V, Chakrabarti K, Bultel A, Tennyson J, Schneider I F and Mezei J Z 2021 *J. Appl. Phys.* **129** 053303

Al-Refaie A F and Tennyson J 2017 *Comput. Phys. Commun.* **221** 53–62

Allan M 1985 *J. Phys. B: At. Mol. Opt. Phys.* **18** 4511–7

Allan M 2010 *Phys. Rev.* A **81** 042706

Antony B K, Joshipura K N, Mason N J and Tennyson J 2004 *J. Phys. B: At. Mol. Opt. Phys.* **37** 1689–97

Ayouz M, Faure A, Tennyson J, Tudorovskaya M and Kokoouline V 2021 *Atoms* **9** 62

Baluja K L, Noble C J and Tennyson J 1985 *J. Phys. B: At. Mol. Phys.* **18** L851–5

Bardsley J N 1968 *J. Phys. B: At. Mol. Phys.* **1** 365–80

Bartschat K 1998 *Comput. Phys. Commun.* **114** 168–82

Bartschat K, Brown A, van der Hart H W, Colgan J and Scott N S 2020 *J. Phys. B: At. Mol. Opt. Phys.* **53** 192002

Bartschat K and Kushner M J 2016 *Proc. Natl Acad. Sci.* **113** 7026–34

Benda J, Gorfinkiel J D, Mašín Z, Armstrong G S J, Brown A C, Clarke D D A, van der Hart H W and Wragg J 2020 *Phys. Rev.* A **102** 052826

Benda J and Mašín Z 2021 *Sci. Rep.* **11** 11686

Blanco F, Ellis-Gibbings L and García G 2016 *Chem. Phys. Lett.* **645** 71–75

Boudaïffa B, Cloutier P, Hunting D, Huels M A and Sanche L 2000 *Science* **287** 1658–60

Brambila D S, Harvey A G, Mašín Z, Gorfinkiel J D and Smirnova O 2015 *J. Phys. B: At. Mol. Opt. Phys.* **48** 245101

Bray I and Stelbovics A T 1992 *Phys. Rev.* A **46** 6995–7011

Breit G and Wigner E 1936 *Phys. Rev.* **49** 519–31

Brigg W J, Tennyson J and Plummer M 2014 *J. Phys. B: At. Mol. Opt. Phys.* **47** 185203

Brown A C, Armstrong G S J, Benda J, Clarke D D A, Wragg J, Hamilton K R, Mašín Z, Gorfinkiel J D and van der Hart H W 2020 *Comput. Phys. Commun.* **250** 107062

Brunger M J and Buckman S J 2002 *Phys. Rep.* **357** 215–458

Brunton J R *et al* 2013 *J. Phys. B: At. Mol. Opt. Phys.* **46** 245203

Burke P G 2011 *R-Matrix Theory of Atomic Collisions: Application to Atomic, Molecular and Optical Processes* (Springer)

Burke V M and Noble C J 1995 *Comput. Phys. Commun.* **85** 471–500

Celiberto R, Janev R K, Wadehra J M and Tennyson J 2012 *Chem. Phys.* **398** 206–13

Cernicharo J, Liu X W, Gonzalez-Alfonso E, Cox P, Barlow M J, Lim T and Swinyard M B 1997 *Astrophys. J.* **483** L65

Chung H K, Braams B J, Bartschat K, Császár A G, Drake G W F, Kirchner T, Kokoouline V and Tennyson J 2016 *J. Phys. D: Appl. Phys.* **49** 363002

Condon E U 1928 *Phys. Rev.* **32** 858–72

Cooper B *et al* 2019 *Atoms* **7** 97

Crawford O H, Dalgarno A and Hays P B 1967 *Mol. Phys.* **13** 181–92

da Costa R F, Varella M T d N, Bettega M H F and Lima M A P 2015 *Eur. Phys. J.* D **69** 159

Darby-Lewis D, Mašín Z and Tennyson J 2017 *J. Phys. B: At. Mol. Opt. Phys.* **50** 175201

Darby-Lewis D, Tennyson J, Yurchenko S N and Lawson K D 2020 *J. Phys. B: At. Mol. Opt. Phys.* **53** 135202

Davis J U Jr and Sommerfeld T 2021 *Eur. Phys. J.* D **75** 316

Deutsch H, Becker K, Matt S and Märk T D 2000 *Int. J. Mass Spec.* **197** 37

dos Santos S F, Ngassam V, Ore A E and Larson A 2016 *Phys. Rev.* A **94** 022702

Dubernet M L *et al* 2013 *Astron. Astrophys.* **553** A50

Dubernet M L *et al* 2024 *Astron. Astrophys.* **683** A40

Fabrikant I I, Eden S, Mason N J and Fedor J Arimondo E, Lin C C and Yelin S F 2017 *Adv. At. Mol. Opt. Phys.* **66** 545–657

Falcetta M F, Fair M C, Slimak S R, Jordan K D and Sommerfeld T 2023 *Phys. Chem. Chem. Phys.* **25** 31028–39

Falkowski A G, da Costa R F, Lima M A P, de ACadena A, Pocoroba R, Jones R, Mathur M, Childers J G, Khakoo M A and Kossoski F 2023 *J. Chem. Phys.* **159** 194301

Faure A, Gorfinkiel J D, Morgan L A and Tennyson J 2002 *Comput. Phys. Commun.* **144** 224–41

Faure A, Gorfinkiel J D and Tennyson J 2004a *Mon. Not. R. Astron. Soc.* **347** 323–33

Faure A, Gorfinkiel J D and Tennyson J 2004b *J. Phys. B: At. Mol. Opt. Phys.* **37** 801–7

Faure A and Tennyson J 2001 *Mon. Not. R. Astron. Soc.* **325** 443–8

Faure A and Tennyson J 2002 *J. Phys. B: At. Mol. Opt. Phys.* **35** 1865–73

Friedman R S and Jamieson M J 1995 *Comput. Phys. Commun.* **85** 231–8

Fujimoto M M, Brigg W J and Tennyson J 2012 *Eur. Phys. J.* D **66** 204

Gailitis M 1976 *J. Phys. B: At. Mol. Phys.* **9** 843

Gianturco F A and Jain A 1986 *Phys. Rev.* **143** 347–425

Gorfinkiel J D and Ptasinska S 2017 *J. Phys. B: At. Mol. Opt. Phys.* **50** 182001

Gorfinkiel J D and Tennyson J 2004 *J. Phys. B: At. Mol. Opt. Phys.* **37** L343–50

Gorfinkiel J D and Tennyson J 2005 *J. Phys. B: At. Mol. Opt. Phys.* **38** 1607–22

Graves V, Cooper B and Tennyson J 2021 *J. Chem. Phys.* **154** 114104

Halmová G and Tennyson J 2008 *Phys. Rev. Lett.* **100** 213202

Hamilton J R, Tennyson J, Huang S and Kushner M J 2017 *Plasma Sources Sci. Technol.* **26** 065010

Hara S 1967 *J. Phys. Soc. Jpn.* **22** 710–8

Hazi A U 1979 *Phys. Rev.* A **19** 920–2

Huang S, Volynets V, Hamilton J R, Lee S, Song I C, Lu S, Tennyson J and Kushner M J 2017 *J. Vac. Sci. Technol.* A **35** 031302

Huang S, Volynets V, Hamilton J R, Nam S K, Song I C, Lu S, Tennyson J and Kushner M J 2018 *J. Vac. Sci. Technol.* A **36** 021305

Jain A 1987 *J. Chem. Phys.* **86** 1289–300

Jimenez-Serra I, Martin-Pintado J, Viti S, Martin S, Rodriguez-Franco A, Faure A and Tennyson J 2006 *Astrophys. J.* **650** L135–8

Johnstone W M, Brunger M J and Newell W R 1999 *J. Phys. B: At. Mol. Opt. Phys.* **32** 5779–88

Jones M and Tennyson J 2010 *J. Phys. B: At. Mol. Opt. Phys.* **43** 045101

Jung K, Antoni T, Muller R, Kochem K H and Ehrhardt H 1982 *J. Phys. B: At. Mol. Phys.* **15** 3535

Jungen C (ed) 1996 *Molecular Applications of Quantum Defect Theory* (Taylor and Francis)

Kadokura R, Loreti A, Köver A, Faure A, Tennyson J and Laricchia G 2019 *Phys. Rev. Lett.* **123** 033401

Kalosi A *et al* 2022 *Phys. Rev. Lett.* **128** 183402

Karwasz G P, Song M Y, Cho H, Kokoouline V and Tennyson J 2023 *Eur. Phys. J.* D **77** 105
Kaur S, Baluja K L and Tennyson J 2008 *Phys. Rev.* A **77** 032718
Kim Y K 2001 *Phys. Rev.* A **64** 032713
Kim Y K and Rudd M E 1994 *Phys. Rev.* A **50** 3954
Laporta V, Cassidy C M, Tennyson J and Celiberto R 2012 *Plasma Sources Sci. Technol.* **21** 045005
Laporta V, Little D A, Celiberto R and Tennyson J 2014 *Plasma Sources Sci. Technol.* **23** 065002
Laporta V, Schneider I F and Tennyson J 2020 *Plasma Sources Sci. Technol.* **20** 10LT01
Larson A, Stenrup M and Orel A E 2012 *Phys. Rev.* A **85** 042702
Larsson M and Orel A E 2008 *Dissociative Recombination of Molecular Ions* (Cambridge University Press)
Levinson N 1949 *Kgl. Danske Videnskab Selskab. Mat. Fys. Medd.* **25** 29
Lima M A P, Gibson T L, Huo W M and McKoy V 1985 *J. Phys. B: At. Mol. Opt. Phys.* **18** L865–70
Little D A, Chakrabarti K, Schneider I F and Tennyson J 2014 *Phys. Rev.* A **90** 052705
Little D A and Tennyson J 2013 *J. Phys. B: At. Mol. Opt. Phys.* **46** 145102
Little D A and Tennyson J 2014 *J. Phys. B: At. Mol. Opt. Phys.* **47** 105204
Little D A, Tennyson J, Plummer M and Sunderland A 2017 *Comput. Phys. Commun.* **215** 137–48
Liu X, Shemansky D E, Ahmed S M, James G K and Ajello J M 1998 *J. Geophys. Res. Atmos.* **103** 26739–58
Maddern T M, Hargreaves L R, Francis-Staite J R, Brunger M J, Buckman S J, Winstead C and Mckoy V 2008 *Phys. Rev. Lett.* **100** 063202
Märk T D and Egger F 1977 *J. Chem. Phys.* **67** 2629–35
Mašín Z, Benda J, Gorfinkiel J D, Harvey A G and Tennyson J 2020 *Comput. Phys. Commun.* **249** 107092
Mašín Z, Benda J, Harvey A G, Al-Refaie A, Gorfinkiel J D and Tennyson J 2019 Ukrmol+: Ukrmol-in *Zenodo* http://dx.doi.org/10.5281/zenodo.2630496
Mašín Z and Gorfinkiel J D 2014 *J. Phys.: Conf. Ser.* **490** 012090
Mebel A M, Lin S H and Pinnaduwage L A 1998 *Chem. Phys. Lett.* **285** 114
Meltzer T, Tennyson J, Mašín Z, Zammit M C, Scarlett L H, Fursa D V and Bray I 2020 *J. Phys. B: At. Mol. Opt. Phys.* **53** 145204
Morgan L A 1984 *Comput. Phys. Commun.* **31** 419–22
Morgan L A 1991 *J. Phys. B: At. Mol. Opt. Phys.* **24** 4649
Morgan L A, Gillan C J, Tennyson J and Chen X 1997 *J. Phys. B: At. Mol. Opt. Phys.* **30** 4087–96
Nestmann B M, Nesbet R K and Peyerimhoff S D 1991 *J. Phys. B: At. Mol. Opt. Phys.* **24** 5133–49
Nestmann B M and Peyerimhoff S D 1990 *J. Phys. B: At. Mol. Opt. Phys.* **23** L773–7
Norcross D W and Padial N T 1982 *Phys. Rev.* A **25** 226–38
Orel A E and Kulander K C 1993 *Phys. Rev. Lett.* **71** 4315–8
Padial N T, Norcross D W and Collins L A 1981 *J. Phys. B: At. Mol. Opt. Phys.* **14** 2901–9
Pitchford L C *et al* 2017 *Plasma Proc. Polym.* **14** 1600098
Rabadán I, Sarpal B K and Tennyson J 1998 *J. Phys. B: At. Mol. Opt. Phys.* **31** 2077–90
Ramsauer C 1921 *Ann. Phys., Lpz.* **369** 513–40
Rescigno T N, McCurdy C W, Orel A E and Lengsfield B H 1995 *Computational Methods For Electron-Molecule Collisions* (*Workshop on Comparative Study of Current Methodologies in Electron-Molecule Scattering, Harvard Smithsonian Ctr Astrophys, Inst Theoret Atom & Molec Phys*) ed W M Huo and F A Gianturco (Plenum) pp 1–44
Sanche L 2009 *Chem. Phys. Lett.* **474** 1–6
Sanna N and Gianturco F A 1998 *Comput. Phys. Commun.* **114** 142–67
Sarpal B K, Tennyson J and Morgan L A 1994 *J. Phys. B: At. Mol. Opt. Phys.* **27** 5943–53
Scarlett L H, Boyle D K, Zammit M C, Ralchenko Y, Bray I and Fursa D V 2022 *At. Data Nucl. Data Tables* **148** 101534
Scarlett L H, Fursa D V, Zammit M C, Bray I, Ralchenko Y and Davie K D 2021 *At. Data Nucl. Data Tables* **137** 101361
Scarlett L H, Fursa V D, Zammit M C, Bray I and Ralchenko Y 2021 *At. Data Nucl. Data Tables* **139** 101403
Scarlett L H, Jong E, Odelia S, Zammit M C, Ralchenko Y, Schneider B I, Bray I and Fursa V D 2023 *At. Data Nucl. Data Tables* **151** 101573
Scarlett L H, Savage J S, Fursa V D, Bray I, Zammit M C and Schneider I B 2021 *Phys. Rev.* A **103** 032802
Schneider B I and Collins L A 1985 *J. Phys. B: At. Mol. Opt. Phys.* **18** L857–63
Seaton M J 1983 *Rep. Prog. Phys.* **46** 167
Shafir D *et al* 2009 *Phys. Rev. Lett.* **102** 223202
Smith F T 1960 *Phys. Rev.* **114** 349–56
Snoeckx R, Tennyson J and Cha M S 2023 *Plasma Sources Sci. Technol.* **32** 115020
Song M Y, Cho H, Karwasz G P, Kokoouline V and Tennyson J 2023 *J. Phys. Chem. Ref. Data* **52** 023104
Stibbe D T and Tennyson J 1997 *Phys. Rev. Lett.* **79** 4116–9
Stibbe D T and Tennyson J 1998a *J. Phys. B: At. Mol. Opt. Phys.* **31** 815–44
Stibbe D T and Tennyson J 1998b *New J. Phys.* **1** 2
Stibbe D T and Tennyson J 1999 *Chem. Phys. Lett.* **308** 532–6
Su H, Cheng X, Cooper B, Tennyson J and Zhang H 2022 *Phys. Rev.* A **105** 062824
Takatsuka K and McKoy V 1981 *Phys. Rev.* A **24** 2473–80
Tanaka H, Brunger M J, Campbell L, Kato H, Hoshino M and Rau A R P 2016 *Rev. Mod. Phys.* **88** 025004
Tennyson J 1988 *J. Phys. B: At. Mol. Opt. Phys.* **21** 805–16
Tennyson J 1996a *J. Phys. B: At. Mol. Opt. Phys.* **29** 1817–28
Tennyson J 1996b *J. Phys. B: At. Mol. Opt. Phys.* **29** 6185–201
Tennyson J 1997 *Comput. Phys. Commun.* **100** 26–30
Tennyson J 2004 *J. Phys. B: At. Mol. Opt. Phys.* **37** 1061–71
Tennyson J 2010 *Phys. Rep.* **491** 29–76
Tennyson J *et al* 2022 *Plasma Sources Sci. Technol.* **31** 095020
Tennyson J and Noble C J 1985 *J. Phys. B: At. Mol. Phys.* **18** 155–65
Thümmel H T, Nesbet R K and Peyerimhoff S D 1992 *J. Phys. B: At. Mol. Opt. Phys.* **25** 4553–79
Toshima N, Ishihara T and Eichler J 1987 *Phys. Rev.* A **36** 2659–66
Trevisan C S, Orel A E and Rescigno T N 2006 *J. Phys. B: At. Mol. Opt. Phys.* **39** L255
UK R-matrix community 2021 Ukrmol+: Ukrmol-out *Zenodo* http://dx.doi.org/10.5281/zenodo.5799134
Volkov M V, Elander N, Yarevsky E and Yakovlev S L 2009 *Europhys. Lett.* **85** 30001
Werner H J *et al* 2020 *J. Chem. Phys.* **152** 144107
Werner H J, Knowles P J, Knizia G, Manby F R and Schütz M 2012 *WIREs Comput. Mol. Sci.* **2** 242–53
Wigner E P and Eisenbud L 1947 *Phys. Rev.* **72** 29–41
Yoon J S, Song M Y, Han J M, Hwang S H, Chang W S, Lee B and Itikawa Y 2008 *J. Phys. Chem. Ref. Data* **37** 913–31
Yoshimine M 1973 *J. Comput. Phys.* **11** 449–54
Zammit M C, Fursa D V, Savage J S and Bray I 2017 *J. Phys. B: At. Mol. Opt. Phys.* **50** 123001
Zhang R, Faure A and Tennyson J 2009 *Phys. Scr.* **80** 015301
Zhang R, Galiatsatos P G and Tennyson J 2011 *J. Phys. B: At. Mol. Opt. Phys.* **44** 195203